



Hetero-deformation induced (HDI) hardening does not increase linearly with strain gradient

Y.F. Wang^a, C.X. Huang^{a,*}, X.T. Fang^b, H.W. Höppel^c, M. Göken^c, Y.T. Zhu^{b,d,**}

^a School of Aeronautics and Astronautics, Sichuan University, Chengdu 610065, China

^b Department of Materials Science and Engineering, North Carolina State University, Raleigh, NC 27695, USA

^c Department of Materials Science and Engineering, Institute I: General Materials Properties, Friedrich-Alexander University of Erlangen-Nürnberg, Martensstr. 5, 91058 Erlangen, Germany

^d Nano and Heterogeneous Materials Center, School of Materials Science and Engineering, Nanjing University of Science and Technology, Nanjing 210094, China

ARTICLE INFO

Article history:

Received 22 June 2019

Received in revised form 9 August 2019

Accepted 19 August 2019

Available online 27 August 2019

Keywords:

Hetero-deformation induced stress

Heterostructures

Interface

Strain gradient

Geometrically necessary dislocations

ABSTRACT

Hetero-deformation induced (HDI) hardening has been attributed to geometrically necessary dislocations (GNDs) that are needed to accommodate strain gradient near the interfaces of heterostructured domains. Here we report that HDI hardening does not increase linearly with increasing strain gradient in the interface-affected zone. This is because some GND pileups may be absorbed by the interface and consequently does not contribute to HDI hardening with increasing strain gradient. Higher mechanical incompatibility across interface produces higher strain gradient. The strain gradient-dependent strengthening effect of heterostructured interface mainly originates from the development of HDI stress.

© 2019 Acta Materialia Inc. Published by Elsevier Ltd. All rights reserved.

Heterostructured metals and alloys have been reported to possess exciting potential of overcoming the strength–ductility tradeoff by introducing high-density of heterostructured domain interfaces [1–13]. These domain interfaces are different from grain boundaries and twin boundaries in conventional homogeneous materials. There are dramatic differences in strength and strain hardening capability across these interfaces [1–3,7–9]. Hetero-deformation caused by this mechanical incompatibility can introduce strain gradient near the interfaces [2–4,8,11]. As suggested by the strain gradient plasticity theory in micromechanics, pileup of geometrically necessary dislocations (GNDs) is needed to accommodate the plastic strain gradient [14,15]. These GNDs are expected to produce back stress strengthening and hardening, in addition to the isotropic strengthening caused by the increase of total dislocation density [1,2,16,17]. It was recently realized that the terms of back stress strengthening and hardening cannot accurately describe the real physics of what occurred across the interface, because GND pileups produces not only back stress in the soft domains, but also forward stress in the hard domains [18]. Back stress and forward stress are conjugated long-range internal stresses with opposite directions, which collectively affect flow stress during the unloading and reloading. Therefore, “back stress” measured from the mechanical

testing (e.g. unloading–reloading [9,19]) was renamed hetero-deformation induced (HDI) stress by Zhu and Wu [18] to accurately describe the extra strain hardening in heterostructured materials [2–4,19–21].

It was assumed in the gradient plasticity theory [14,15] that the GND density and gradient are quantitatively related to the strain gradient near the interface. GND gradient was found to indeed exist near domain interfaces [12]. Strain gradient was measured and an interface affected zone (IAZ) was found near the domain interface [11]. These earlier works led to the belief that the HDI hardening increases with strain gradient and a quantitative relationship exists between them. However, a recent in-situ transmission electron microscopy (TEM) examination revealed that Frank-Read sources and dislocation pileups were dynamically formed and disappeared during tensile test [22], which suggested that the GND density and gradient may not be quantitatively related to the strain gradient. Consequently, the HDI hardening may not be quantitatively related to the strain gradient. To clarify this issue, it is essential to compare the developments of the strain gradient around interface and the associated HDI stress.

In this study, microscale digital image correlation (μ -DIC) was used to characterize the evolution of strain gradient in the interface-affected zone (IAZ) during tensile testing. The result was compared with the evolution of HDI hardening, which was measured by unloading–reloading approach [2,9,19]. The comparison revealed that the HDI hardening does not have a linear relationship with increasing strain gradient in the IAZ.

* Corresponding author.

** Correspondence to: Y.T. Zhu, Department of Materials Science and Engineering, North Carolina State University, Raleigh, NC 27695, USA.

E-mail addresses: chxhuang@scu.edu.cn (C.X. Huang), ytzhu@ncsu.edu (Y.T. Zhu).

Three types of laminate samples stacked with alternate sequences of copper and brass (Cu-10 wt% Zn), copper and brass (Cu-30 wt% Zn), copper and copper were accumulatively roll-bonded (ARB) to a layer thickness of $\sim 62 \mu\text{m}$ at room temperature. The as-received copper-brass (Cu-10 wt% Zn) laminates were further rolled to a layer thickness of $31 \mu\text{m}$, $15 \mu\text{m}$, or $7.5 \mu\text{m}$. Thereafter, all laminates were annealed at 220°C for 2 h so that recrystallization occurs in Cu layers but not in Cu–Zn alloy layers. The Cu layers in as-annealed laminates are characterized with fully recrystallized coarse grains (CG), while the Cu–Zn alloy layers exhibit severely deformed nanostructures (NS) [11,12]. For simplicity, three types of laminates were labeled as CG/NS_{10Zn}, CG/NS_{30Zn}, and CG/CG, respectively, in which CG represents coarse-grained Cu layer.

Hardness was measured using an MTS Nanoindenter XP equipped with a Berkovich pyramid indenter. As shown in Fig. 1(a), sharp interfaces with significant hardness incompatibility in adjacent domains exist in heterogeneous CG/NS_{10Zn} and CG/NS_{30Zn} laminates, while no hardness difference across the interfaces in CG/CG sample.

Dog-bone-shaped small sample with the gauge length parallel to the rolling direction was prepared for μ -DIC strain measurement. Refined speckle pattern prepared by electrochemical etching was recorded by secondary electron imaging. The detailed test procedures are reported in our previous work [11]. Fig. 1(b–d) present the distribution of strain $-\varepsilon_x$ across interfaces. The strain distribution is averaged along the interface and plotted as a function of distance from an interface (Fig. 1(e)), which provides insights on the statistical nature of strain distribution near the interface. Obviously, interface-affected zones (IAZs) spanning $\sim 10 \mu\text{m}$ with a negative strain gradient are formed at heterostructured interfaces in CG/NS_{10Zn} and CG/NS_{30Zn} laminates. In contrast, strain ε_x in CG/CG sample evolves uniformly across the homogeneous interface (the green curve in Fig. 1(e)). Comparing Fig. 1(a) with (e) reveals that the magnitude of strain gradient increases with higher mechanical incompatibility.

The negative gradient of strain ε_x was caused by the gradient distribution of dynamically generated Frank-Read sources near the heterostructured interface [22]. The mechanical incompatibility leads to synergistic constraint between heterogeneous domains during

tension, which changes the local stress state and causes stress concentration near the interface [4,23,24]. The closer to the interface, the higher probability to activate Frank-Read sources because of the higher local stresses. The Frank-Read sources are essentially dislocation segments with various lengths between dislocation jogs, which are formed by the interaction of intersecting dislocations gliding on different slip planes [22,25]. Therefore, it is logical to expect that sites closer to interface should experience more dislocation activities, and thus have higher measurable strain. Higher mechanical incompatibility induces larger stress gradient near interface, which will cause more intense Frank-Read source gradient. This is the reason why the strain gradient at the CG/NS_{30Zn} interface is much steeper than that at the CG/NS_{10Zn} interface (Fig. 1(a) and (e)).

Fig. 2(a) shows the statistical evolution of strain ε_x in CG/NS_{10Zn} laminate with increasing applied strain ε_y . The ratio of the height (H) and the width at half height (W) of strain concentration peak, H/W , can be used to quantify the mean intensity of strain gradient $|d\varepsilon_x/dx|$ in IAZ. As shown in Fig. 2(b), the mean $|d\varepsilon_x/dx|$ in the IAZ increases almost linearly with applied strain. In other words, the strain gradient in the IAZ increases linearly with applied strain. As discussed latter, this can be attributed to the formation and deactivation of dislocation pileups near the heterostructured interface.

Since the width of the IAZ is not affected by layer thickness until adjacent IAZs start to overlap [11,12], the volume fraction of IAZ (V_{IAZ}) is primarily determined by the interface density. The V_{IAZ} in the four groups of CG/NS_{10Zn} samples with layer thicknesses of $62 \mu\text{m}$, $31 \mu\text{m}$, $15 \mu\text{m}$ and $7.5 \mu\text{m}$ are approximately 16.8%, 33.6%, 69.5% and 100%, respectively. These samples are used to deduce the strain gradient-related strengthening effects of heterostructured interfaces. Tensile samples with a gauge length of 12 mm and a width of 2 mm were machined for both uniaxial and loading–unloading–reloading (LUR) tensile tests. HDI stress is deduced from hysteresis loops (Fig. 3(a)) using the procedure that was used to measure the “back stress” [2,9]. As shown in Fig. 3(b), the measured HDI stress (σ_{HDI}) increases with applied strain, and the sample with higher V_{IAZ} has higher HDI stress.

Note that microscopically plastic strain produced by dislocations is intrinsically heterogeneous in polycrystalline materials [26]. The back

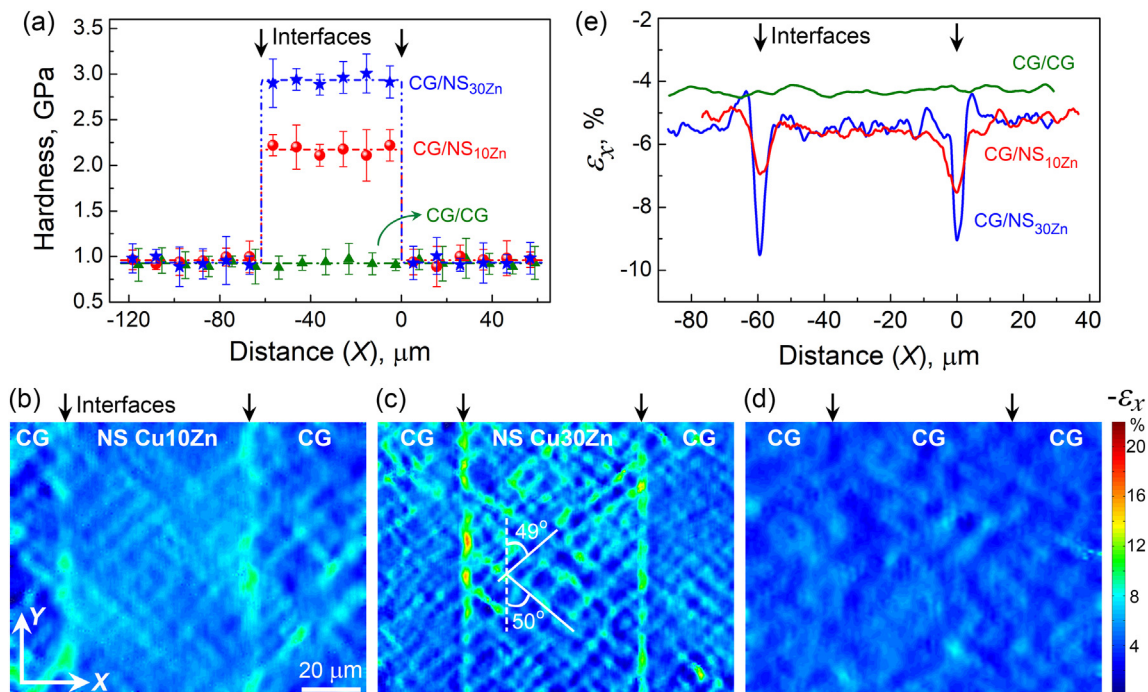


Fig. 1. (a) Hardness profiles of three types of laminates. Every data point was averaged from 5 nanoindentations. The $-\varepsilon_x$ strain maps at the tensile strain of $\sim 10\%$: (b) CG/NS_{10Zn} [11], (c) CG/NS_{30Zn} and (d) CG/CG. In the coordinate, Y is the tensile direction, and X is the sample thickness direction perpendicular to interface. (e) The distribution of statistical average strain ε_x as a function of distance from the right interface. The white lines in (c) mark the shear banding direction.

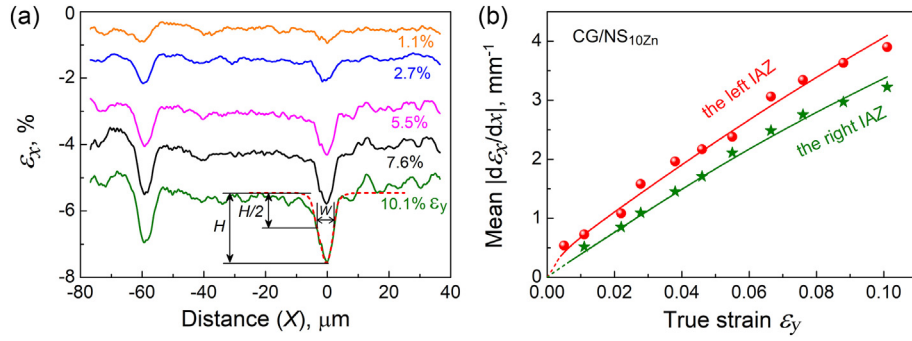


Fig. 2. Evolution of strain ε_x in CG/NS_{10Zn} with increasing applied strain ε_y : (a) statistical averaged distribution [11], (b) the mean strain gradient $|d\varepsilon_x/dx|$ in IAZ. The intensity (H) and the width at half intensity (W) of strain concentration peak at interface are extracted from the Gaussian fitting (red dotted line). Mean $|d\varepsilon_x/dx|$ is approximately equal to the ratio H/W .

stress and forward stress can also be built up in homogeneous materials due to the non-uniform dislocation pileups against grain boundary or dislocation walls [16]. For example, pronounced hysteresis effects were observed in work-hardened polycrystalline and freestanding NS samples [9,16,25]. Therefore, the above measured HDI stress at a certain applied strain should be the total σ_{HDI} of laminate sample which can be expressed as

$$\sigma_{HDI} = (V_{NS}\sigma_{HDI,NS} + V_{CG}\sigma_{HDI,CG}) + V_{IAZ}\sigma_{HDI,IAZ}, \quad (1)$$

where $\sigma_{HDI,NS}$ and $\sigma_{HDI,CG}$ are the HDI stress intrinsic to NS and CG components, respectively. $\sigma_{HDI,IAZ}$ represents the HDI stress developed from per unite IAZ volume fraction, i.e., the HDI stress induced by the heterodeformation in the IAZ. The contribution of these HDI stress components in a laminate can be evaluated basing on the volume fraction of their origin.

Fig. 3(c) shows the fitting of the total σ_{HDI} as a function of V_{IAZ} according to the linear relationship described in Eq. (1). As shown, the slope and intercept of the fitting line represent the magnitude of $\sigma_{HDI,IAZ}$ and $V_{NS}\sigma_{HDI,NS} + V_{CG}\sigma_{HDI,CG}$ at a certain applied strain, respectively. Fig. 3(d) shows the evolution of the $\sigma_{HDI,IAZ}$ with increasing applied strain. Surprisingly, the $\sigma_{HDI,IAZ}$ increased quickly at the early strain stage, and then slowed down at a tensile strain of ~2%. Note that the derived $\sigma_{HDI,IAZ}$ is the upper limit of HDI stress in a laminate with non-overlapping IAZs. The evolution of $\sigma_{HDI,IAZ}$ with increasing applied strain (Fig. 3(d)) is different from the linear evolution of strain gradient intensity (Fig. 2(b)), which indicates that the HDI stress in the IAZ does not increase linearly with increasing strain gradient in the IAZ. This observation contradicts earlier theory and assumption that the development of HDI stress depends proportionally on the evolution strain gradient [1,11,12,21].

The development of HDI stress from IAZ is caused by the piling up and accumulation of GNDs [18]. Specifically, the spatial gradient of

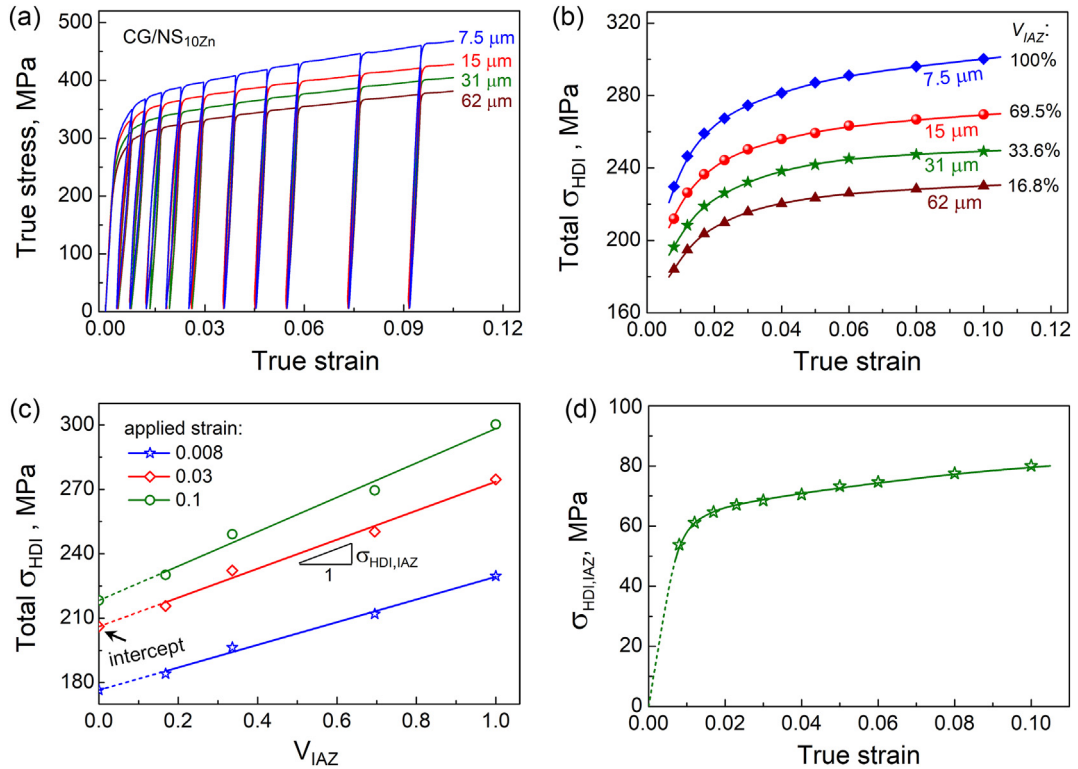


Fig. 3. Deduction of the HDI stress developed from per unit volume fraction of IAZ ($\sigma_{HDI,IAZ}$). (a) LUR curves and hysteresis loops of CG/NS_{10Zn} laminates with different layer thickness, i.e., CG/NS_{10Zn} samples with varying volume fraction of IAZ (V_{IAZ}). (b) Total σ_{HDI} of laminates. (c) Linear fitting of the total σ_{HDI} as a function of V_{IAZ} , showing the deduction of $\sigma_{HDI,IAZ}$ at a certain strain. (d) Evolution of $\sigma_{HDI,IAZ}$ with applied strain.

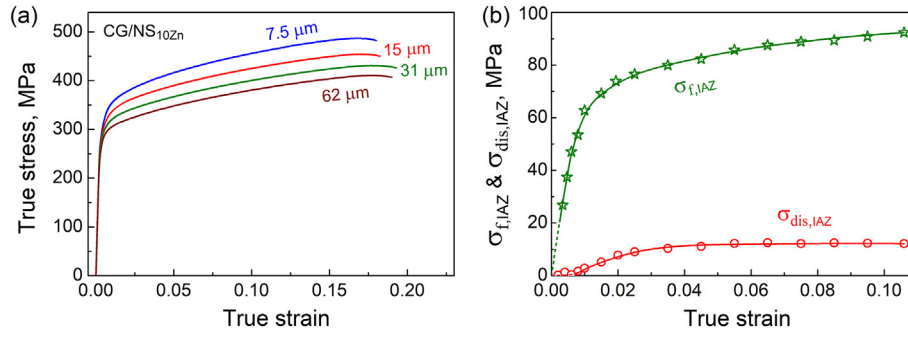


Fig. 4. (a) Uniaxial tensile response of CG/NS_{10Zn} laminates [11]. (b) The total strengthening effect ($\sigma_{f,IAZ}$) and the dislocation strengthening ($\sigma_{dis,IAZ}$) developed from per unit volume fraction of IAZ.

GND density ($\nabla\rho_{GND}$) contributes to the net long-range internal stress. The HDI stress at a specific position can be in theory calculated by integrating the stress field of each individual GND as $\sigma_{HDI} \propto \nabla \rho_{GND}$ [21,25,27–29]. This expression can be further rephrased as $\sigma_{HDI} \propto \nabla \eta$ if one assumes that ρ_{GND} is proportional to the strain gradient η [14,15]. Accordingly, during straining, the HDI stress caused by GND pileups in local strain gradient zone should develop proportionally with the evolution of strain gradient intensity. In other words, an increase in strain gradient should lead to a constant increase of HDI stress. This is why HDI stress was assumed or hinted to increase linearly with strain gradient intensity in earlier works [1,11,12,21].

The fast increase of HDI hardening before 2% applied strain (Fig. 3(d)) indicates that a quick GND piling-up process at the elastic-plastic transition and low-plastic strain stages [18]. With further tensile straining, the dramatic slowdown of HDI hardening implies that the piling-up slowed down. Logically, this could be caused by the slowdown of strain gradient increase. However, Fig. 2(b) shows that strain gradient in the IAZ increased linearly with applied strain during the entire tensile testing. In other words, the GND accumulation slowed down after 2% applied strain in the IAZ despite the continuous increase in the strain gradient. This can be attributed to the dynamic formation and disappearance of GND pileups in the IAZ [22].

As revealed by in-situ TEM observation [22], the piling up of GNDs near interface is accompanied with the formation and activation of Frank-Read source, which may be absorbed by the heterostructured interface as the associated source becomes deactivated in subsequent straining. Disappeared GND pileups took away their contribution to HDI stress but left strain in the slipping path. At the large strain stage, the new formation and disappearance of pileups tend to reach a dynamic saturation, leading to a significant slowing down of HDI stress (Fig. 3(d)) but a continuous increase of strain accumulation near interface (Fig. 2(b)). In short, the primary physics behind the non-proportional relationship between the developments of HDI stress and strain gradient is the decoupling of GNDs accumulation and strain gradient development in IAZs at the large plastic strain stage.

The true stress-strain curves of CG/NS_{10Zn} samples are plotted in Fig. 4(a). As shown, the flow stress increases with decreasing layer thickness. The measured flow stress (σ_f) of laminates at a certain applied strain can be expressed as

$$\sigma_f = (V_{NS}\sigma_{f,NS} + V_{CG}\sigma_{f,CG}) + V_{IAZ}\sigma_{f,IAZ}, \quad (2)$$

where $\sigma_{f,NS}$ and $\sigma_{f,CG}$ are the flow stress intrinsic to NS and CG components, respectively. $\sigma_{f,IAZ}$ is the flow stress developed from per unit IAZ volume fraction, i.e., the extra strengthening caused by GND pileups in an IAZ. Similar to the fitting process shown in Fig. 3(c), the $\sigma_{f,IAZ}$ at certain strain can be extracted by extracting the slope of the linear relationship between σ_f and V_{IAZ} . The green curve in Fig. 4(b) shows the evolution of $\sigma_{f,IAZ}$ with applied strain.

Since the piling up of GNDs in IAZ can also produce extra dislocation strengthening ($\sigma_{dis,IAZ}$), i.e., Taylor strengthening due to the increase of total dislocation density [14], the $\sigma_{f,IAZ}$ is the sum of $\sigma_{HDI,IAZ}$ and $\sigma_{dis,IAZ}$,

$$\sigma_{f,IAZ} = \sigma_{HDI,IAZ} + \sigma_{dis,IAZ}. \quad (3)$$

$\sigma_{dis,IAZ}$ can be deduced by subtracting the $\sigma_{HDI,IAZ}$ from the $\sigma_{f,IAZ}$. Interestingly, $\sigma_{dis,IAZ}$ (the red curve in Fig. 4(b)) is much smaller than $\sigma_{f,IAZ}$, especially at the early strain stage. This indicates that the extra strain hardening in the IAZ primarily comes from the HDI hardening, instead of the isotropic dislocation hardening, especially at the early elastic-plastic stage. This result provides direct evidence to the earlier claim that long-range internal stress dominated extraordinary strengthening and work hardening in heterostructured materials [2,3,9,19].

Note that the parameters $\sigma_{HDI,NS}$ and $\sigma_{f,NS}$ used in Eqs. (1) and (3) may not be equal to the corresponding those in a freestanding NS layer, because the stress state of NS layers in a laminate is modified by the synergistic constraint from neighboring CG layers. As shown in Fig. 1(b) and (c), stable shear bands are dispersed in the NS layer, which helps with accommodating applied strain and retaining uniform elongation [30]. This unique deformation mode did not occur in a freestanding NS counterpart. This observation indicates that the interface effects, $\sigma_{HDI,IAZ}$ and $\sigma_{f,IAZ}$, cannot be simply deduced from the mechanical responses of freestanding components because of the synergistic interactions among different layers [6,23].

In summary, it is found that the mechanical incompatibility induces the formation of IAZ, where negative strain gradient is developed in the direction perpendicular to the interface. The intensity of strain gradient in IAZ increases linearly with applied strain, while the HDI stress developed from the GNDs pileup in IAZ increases quickly at the early strain stage and then slows down to approximate saturation. These are due to the dynamical formation and disappearance of dislocation pileups near interface during straining, and indicate that there is no quantitative relationship between them. Importantly, the strain gradient-related strengthening effect of heterostructured interface is mainly originated from the development of HDI stress, instead of the increase of total dislocation density. This work sheds light on the possibility of enhancing the hetero-deformation induced hardening by architecting heterostructured interface.

Acknowledgements

This work was supported by the National Key Research and Development Program of China (2017YFA0204403), the National Natural Science Foundation of China (Nos. 11672195 and 51931003) and Sichuan Youth Science and Technology Foundation (2016JQ0047). Y.F.W. would like to acknowledge the support from China Scholar Council. Y.T.Z. was funded by the US Army Research Office.

References

- [1] X.L. Wu, Y.T. Zhu, *Mater. Res. Lett.* 5 (2017) 527–532.
- [2] X.L. Wu, M.X. Yang, F.P. Yuan, G.L. Wu, Y.J. Wei, X.X. Huang, Y.T. Zhu, *Proc. Natl. Acad. Sci. U. S. A.* 112 (2015) 14501–14505.
- [3] H.K. Park, K. Ameyama, J. Yoo, H. Hwang, H.S. Kim, *Mater. Res. Lett.* 6 (2018) 261–267.
- [4] X.L. Wu, P. Jiang, L. Chen, F.P. Yuan, Y.T. Zhu, *Proc. Natl. Acad. Sci. U. S. A.* 111 (2014) 7197–7201.
- [5] S.W. Wu, G. Wang, Q. Wang, Y.D. Jia, J. Yi, Q.J. Zhai, J.B. Liu, B.A. Sun, H.J. Chu, J. Shen, P.K. Liaw, C.T. Liu, T.Y. Zhang, *Acta Mater.* 165 (2019) 444–458.
- [6] Y.F. Wang, C.X. Huang, M.S. Wang, Y.S. Li, Y.T. Zhu, *Scr. Mater.* 150 (2018) 22–25.
- [7] Z. Cheng, H.F. Zhou, Q.H. Lu, H.J. Gao, L. Lu, *Science* 362 (2018), eaau1925.
- [8] Z. Cheng, L. Lu, *Scr. Mater.* 164 (2019) 130–134.
- [9] Y.F. Wang, M.X. Yang, X.L. Ma, M.S. Wang, K. Yin, A.H. Huang, C.X. Huang, *Mater. Sci. Eng. A* 727 (2018) 113–118.
- [10] M. Huang, C. Xu, G.H. Fan, E. Maawad, W.M. Gan, L. Geng, F.X. Lin, G.Z. Tang, H. Wu, Y. Du, D.Y. Li, K.S. Miao, T.T. Zhang, X.S. Yang, Y.P. Xia, G.J. Cao, H.J. Kang, T.M. Wang, T.Q. Xiao, H.L. Xie, *Acta Mater.* 153 (2018) 235–249.
- [11] C.X. Huang, Y.F. Wang, X.L. Ma, S. Yin, H.W. Höppel, M. Göken, X.L. Wu, H.J. Gao, Y.T. Zhu, *Mater. Today* 21 (2018) 713–719.
- [12] X.L. Ma, C.X. Huang, J. Moering, M. Ruppert, H.W. Höppel, M. Göken, J. Narayan, Y.T. Zhu, *Acta Mater.* 116 (2016) 43–52.
- [13] J. Wang, A. Misra, *Curr. Opin. Solid State Mater. Sci.* 15 (2011) 20–28.
- [14] H. Gao, Y. Huang, W.D. Nix, J.W. Hutchinson, *J. Mech. Phys. Solids* 47 (1999) 1239–1263.
- [15] J.W. Hutchinson, *Int. J. Solids Struct.* 37 (2000) 225–238.
- [16] H. Mughrabi, *Acta Metall.* 31 (1983) 1367–1379.
- [17] X. Feaugas, *Acta Mater.* 47 (1999) 3617–3632.
- [18] Y.T. Zhu, X.L. Wu, *Mater. Res. Lett.* 7 (2019) 393–398.
- [19] M.X. Yang, Y. Pan, F.P. Yuan, Y.T. Zhu, X.L. Wu, *Mater. Res. Lett.* 4 (2016) 145–151.
- [20] H.H. Lee, J.I. Yoon, H.K. Park, H.S. Kim, *Acta Mater.* 166 (2019) 638–649.
- [21] J.J. Li, G.J. Weng, S.H. Chen, X.L. Wu, *Int. J. Plast.* 88 (2017) 89–107.
- [22] H. Zhou, C.X. Huang, X.C. Sha, L.R. Xiao, X.L. Ma, H.W. Höppel, M. Göken, X.L. Wu, K. Ameyama, X.D. Han, Y.T. Zhu, *Mater. Res. Lett.* 7 (2019) 376–382.
- [23] X.L. Wu, P. Jiang, L. Chen, J.F. Zhang, F.P. Yuan, Y.T. Zhu, *Mater. Res. Lett.* 2 (2014) 185–191.
- [24] Y.F. Wang, M.S. Wang, K. Yin, A.H. Huang, Y.S. Li, C.X. Huang, *Trans. Nonferrous Metals Soc. China* 29 (2019) 588–594.
- [25] F. Momprou, D. Caillard, M. Legros, H. Mughrabi, *Acta Mater.* 60 (2012) 3402–3414.
- [26] B. Bay, N. Hansen, D.A. Hughes, D. Kuhlmann-Wilsdorf, *Acta Metall. Mater.* 40 (1992) 205–219.
- [27] C.J. Bayley, W.A.M. Brekelmans, M.G.D. Geers, *Int. J. Solids Struct.* 43 (2006) 7268–7286.
- [28] L.P. Evers, W.A.M. Brekelmans, M.G.D. Geers, *Int. J. Solids Struct.* 41 (2004) 5209–5230.
- [29] M. Kuroda, V. Tvergaard, *J. Mech. Phys. Solid.* 56 (2008) 1591–1608.
- [30] Y.F. Wang, C.X. Huang, Q. He, F.J. Guo, M.S. Wang, L.Y. Song, Y.T. Zhu, *Scr. Mater.* 170 (2019) 76–80.